Polym. Bull. (2009) 62:209–223
DOI 10.1007/s00289-008-0009-8

ORIGINAL PAPER

Preparation and characterization of branched polyesteramide/mix rare earth oxides composites

Qinghua Chen · Rongguo Chen · Liren Xiao · Qingrong Qian · Wengong Zhang · Xiaoming Fang

Received: 11 August 2008 / Revised: 31 October 2008 / Accepted: 3 November 2008 / Published online: 17 December 2008

Abstract Branched polyester amide containing various amount of mix rare earth oxides (RE_2O_3) were synthesized by in-situ solution condensation of AB_2 monomer synthesized based on the reaction between maleic anhydride and diethanolamine (DEA). The effect of AB_2 monomer self-polycondensation on the RE_2O_3 surface and the properties of synthesized composites were investigated by using Fourier-transform infrared spectra (FT-IR), ultraviolet–visible absorption spectra (UV–vis), X-ray photoelectron spectroscopy, scanning electron microscopy, thermogravimetric analysis and viscosity determination. AB_2 monomer can envelop RE_2O_3 particles as an organic matrix (HBPEA′) by self-polycondensation under the proposed condition. Ionization of surface of RE_2O_3 aggregates can result in the rare earth ionic (RE^{3+}) and the resulting RE^{3+} might coordinate with the organic matrix. Thermal stability of branched polyesteramide can be significantly improved in presence of 5 wt% RE_2O_3, possibly due to the coordination reaction between RE_2O_3 and the active group of the organic matrix.

Keywords Branched polyesteramide · Rare earth oxides · Composites

Q. Chen (✉) · R. Chen · L. Xiao · Q. Qian · W. Zhang (✉) · X. Fang
College of Chemistry and Materials Science,
Institute of Fujian Modified Plastic Research and Develop Technology,
Fujian Normal University, 350007 Fuzhou, China
e-mail: cqhuar@pub5.fz.fj.cn

W. Zhang
e-mail: wgzhang@fjnu.edu.cn

R. Chen
Department of Environment and Equipment Engineering,
Fujian University of Technology, 350007 Fuzhou, China

Introduction

With unique properties that can solve the problems related to processability, property compromises, and compatibility in blends system, hyperbranched polymer (HBP) has a high potential as additives and modifiers in engineering materials [1]. As a small embranchment of HBP, hyperbranched polyesteramide (HBPEA) can be facilely synthesized by introducing commercial monomer and has been excitingly explored in recent years [2–5]. Fortunately, some polymer-system researchful application examples to HBPEA have proven to be successful, such as, incorporation of 3% stearate-modified Hybrane (DSM New Business Development) can markedly enhance the dyeability of polypropylene with C. I. Disperse Blue 56 [6]. A certain HBPEA can afford an advantage in processability, thermal and mechanical properties of polylactide without meeting an embarrassment of property improvement with drastic loss of the general performance [7]. Promisingly, HBPEA may be a kind of novel biodegradable additive, for easy hydrolytic and enzymatic degradation resulted from containing many branching ester bonds [8, 9]. In particular, HBPEA containing the double bond structure can provide some more specificity to be used as a potential UV-response functional additive [10] or UV-curable powder coating [11]. However, from an application point of view, it is unreasonable for expensive HBPEA to be used as additive in general industrial fields, such as plastic and rubber processing.

Compounding inorganic material to HBP seems to be an effective and versatile method to overcome such a high-cost bottleneck, which may offer various possibilities including: (1) tailoring the chemical and physical properties; (2) functionalizing resultant composite [12, 13]; (3) cutting cost. In reality, HBP-inorganic composites have already attracting more and more considerable interest in polymer field, and there are many inorganic materials reported involving HBP-based composites recently, such as Ag [14], Si [15], SiO_2 [16, 17], PbS [18], TiO_2 [19], alumina ceramic [20], carbon black [21], carbon nanofiber [22], montmorillonite [23], attapulgite [24], etc. Whereas, hitherto, to our best knowledge there is no any attention to pay to a certain valuable low-cost rare earth materials, i.e., mix rare earth oxides (RE_2O_3, RE = La, Ce, Pr, Nd, etc.), which can be easily extracted from raw mineral. HBP-based RE_2O_3 composites may be a kind of novel rare composites with the lower cost and multifunction to break the apply dream [25] of HBP due to integrating RE_2O_3 magic properties to HBP unique properties. There are lots of examples for RE_2O_3 to be pleasantly surprised application, for instance, as multi-functional nanoparticle material [26], excellent dopant for oxide ion conductor [27], laser clad coatings [28], active monolith catalysts for methane oxidation [29], and so on. Moreover, in some case, substituting for pure rare oxide, RE_2O_3 application can unexpectedly achieve a better capability/price ratio [30].

In this work, a feasible and relative simple process was developed by compounding HBPEA and RE_2O_3. The resulting HBPEA/RE_2O_3 composites were characterized by Fourier-transform infrared spectra (FT-IR), TGA, X-ray photoelectron spectroscopy (XPS), scanning electron microscopy (SEM), UV–vis spectra and viscosity determination. Meanwhile, the possible interaction between RE_2O_3 and HBPEA in the composites were discussed.

Experimental section

Materials and monomers

RE_2O_3 (La_2O_3 84.90, Ce_2O_3 3.28, Pr_2O_3 0.19, Nd_2O_3 0.24, others 11.39%) with an average diameter of 700–800 nm was provided by Weilinna Co. Ltd., Guandong, China. Diethanolamine (DEA), maleic anhydride (MA), *p*-toluence sulfonic acid (TSA), *N*,*N*-dimethylacetamide (DMAC) and potassium hydroxide (KOH) were purchased from the National Chemical Co. Ltd. All reagents were of analytical reagent grade except for RE_2O_3 which was of commercial product.

Synthesis procedure

Scheme 1 presents preparation procedure for AB_2 monomer (Reaction a), HBPEA (Reaction b) and HBPEA/RE_2O_3 (Reaction d). AB_2 monomer synthesis: in a typical run, 0.1 mol (9.8060 g) MA was dissolved with 30.0 g DMAC in a flask at room temperature. Then 0.1 mol (10.5140 g) crystal DEA heated to be liquid state, was rapidly added into the MA solution. The resultant mixture was stirred with a magnetic stirrer at room temperature to react 2 h, thus AB_2 monomer solution of DMAC was obtained. For structure characterization, the AB_2 specimen film was obtained to be used through casting and evaporating AB_2 solution below 60 °C.

HBPEA/RE_2O_3 composites were synthesized via AB_2 monomer self-polycondensation of "one-step process" on the surface of RE_2O_3 in the presence of TSA as a catalyst. The polycondensation of AB_2 monomer was carried out in a 100 mL three-necked round-bottomed flask equipped with a magnetic stirrer, an circulating bath and a temperature control device, one of whose neck mouth was installed a reflux distillation equipment with water condenser and ventilated a vacuum pump. In a typical run, 48.7683 g the obtained AB_2 monomer solution, 0.0985 g TSA, and calculated amounts of RE_2O_3 according to designed formulae were introduced into the reactor. The system temperature was then maintained at 120 °C, and the vacuum pump was turned on to gained a desired systemic vacuum degree (0.070–0.096 Mpa), under which the H_2O side product would be gradually and continuously

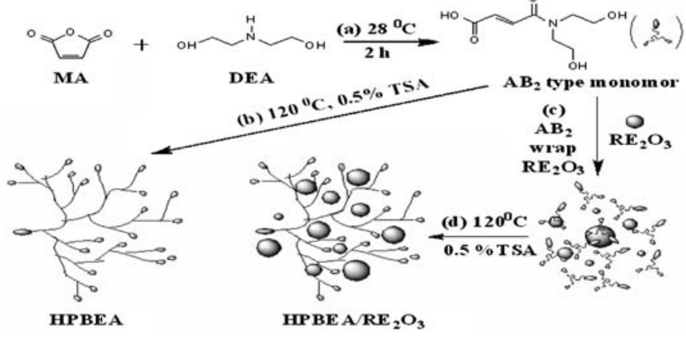

Scheme 1 Preparation procedure for AB_2 monomer, HBPEA/RE_2O_3 and HBPEA

distilled out, so as to conduct the reduced-pressure-distillation polymerization. After 6 h, the reactor was vented and the residual DMAC was subsequently evaporated. Thus a series of ivory-white HBPEA/RE_2O_3 composites were obtained. Partial crude products were dissolved in 30.0 g DMAC, and later filtrated. Resulting sediments were repetitively extracted and rinsed with deionized water, then dried and preserved as RE_2O_3' specimens. And the filtrates were multiplely precipitated in long time by adding mixed solvents of ethylether-acetone (vol. ratio is 1:1). Resulting precipitates were dried in a vacuum oven at 60 °C for 48 h and airtightly preserved as HBPEA′ specimens. For comparison, HBPEA was prepared according to Reaction b whose condition was the same as Reaction d except for there was no RE_2O_3 presence, and purified by precipitation. In addition, RE_2O_3 was mechanically blended with HBPEA at 120 °C in 30.0 g DMAC solvent for 6 h, and then the DMAC was decompressingly evaporated to gained the simple blends (HBPEA + RE_2O_3).

Characterization

FT-IR spectra were recorded on a NICOLET5700 spectrometer, an Origin Peak Fitting Module 7.0 program was used in 3,700–3,100 cm^{-1} and 1,800–1,525 cm^{-1} regions, the initial parameters were obtained from the second derivative spectra, then the interactive procedure and Gaussian type curves were chosen to correct these parameters and compute particular peaks (all correct coefficient > 0.999). SEM micrographs were made on KYKY1000B system for samples coating with gold through sputtering, threshold binarization of the resultant images were gained from a Photoshop7.0 program, and the particle sizes were analyzed with an Image J program. XPS spectra were recorded on a PHI Quantum 2000 Scanning ESCA Microprobe system with the Al K_α X-ray source ($h\upsilon$ = 1 486.6 eV) operating at 5×10^{-8} Pa of vacuum degree or less. The binding energies of the photoelectrons were correlated by the aliphatic hydrocarbon C(1 s) peak at 284.8 eV. Thermal analyses were carried out on a METTLER TGA/SDTA/DSC851 thermal analysis instrument at a heating rate of 10 K/min under nitrogen atmosphere. UV–vis absorption spectra were performed on a VARIAN CARY 50BIO spectrometer with the specimens' ethanol solution of 1×10^{-4} mol/L, all of which were filtrated by employing refined filter cardboard (single membrane, thickness: 3.7 ± 0.2 mm, max aperture ≤0.8 μm). Transmittances of 0.5 g/dL aqueous solution of HBPEA/RE_2O_3 composites and HBPEA + RE_2O_3 blends were conducted using 751-GW UV–vis spectrophotometer at 480 nm wavelength by taking HBPEA aqueous solution as blank specimen. The intrinsic viscosities of HBPEA and HBPEA′ were determined in 0.5 g/dL aqueous solution with an Ubbelhode capillary viscometer at 25.0 °C. The number average molecular weight ($\bar{M}n$) of HBPEA and HBPEA′ were detected according to the literature [31].

Results and discussion

In general, it has been recognized as a more feasible way to synthesize HBP by polycondensation of AB*x* type monomers. However, most AB*x* type monomers are unavailable commercially. Reaction of commercially available AA′ and B′B*x* type monomers can result in the formation of dimers that can be regarded as a new sort of AB*x* monomer, which seems to be a promising strategy for HBP preparation [32].

In the fist step, AB_2 type monomer can be rapidly (2 h) prepared at room temperature (28 ± 2 °C) using MA and DEA. Figure 1 shows representative IR peak separation for AB_2 monomer (possible assignment listed in Table 1), according with characteristic IR absorption feature of dominant amide intermediate product, which contains theoretical structure with one carboxyl and two hydroxyl groups [33]. This method benefits from the fact that the amino group (B′) is more reactive than the hydroxyl (B) toward the carboxylic anhydride, and the reaction of aliphatic second amine and aliphatic anhydride yields an amide acid with multihydroxyl [2, 34, 35].

In the second step, the multihydroxyl amide acid conducted further self-polycondensation as a new AB_2 monomer to yield HBPEA under the proposed condition, which can be identified from the differential IR absorption performance of the intermediate and resultant products. Figure 2 a and b which provides evidence for the chemical structure of the resultant polymers, reveals the representative spectrum of HBPEA which possesses strong absorption bands at 1,729, 1,636, 1,292, 1,170, 1,130 and 1,049 cm^{-1} for tertiary amide-ester group and in 3,250–3,600 cm^{-1} range for hydroxyl group, this indicates that it is an amide-ester compound with multi-hydroxyl groups [10]. Whereas, all the characteristic absorption bands mentioned above are not observed in the AB_2 monomer spectrum.

In the presence of RE_2O_3, the AB_2 monomer can also successfully conduct self-polycondensation on the RE_2O_3 surface to form an organic HBPEA layer. From Fig. 2, we can find that HBPEA/RE_2O_3 (5 wt%) and HBPEA share all the peaks in IR spectra. There are two types of carbonyl absorption peaks, i.e., the amido-carbonyl band at 1,639 cm^{-1} and carboxylic ester carbonyl band at 1,729 cm^{-1}, in both HBPEA/RE_2O_3 and HBPEA. The absorption at 1,729, 1,170 and 1,049 cm^{-1} implies the formation of R–O–C(=O)–R′ ester bonds [36]. Absorption band at around 1,636 cm^{-1} confirms the presence of R–C(=O)–N(R′)$_2$ amide groups [37]. In addition, a shoulder in the region of 3,250–3,600 cm^{-1} attributes to the hydrogen-bonded hydroxyl groups and free hydroxyl groups [38].

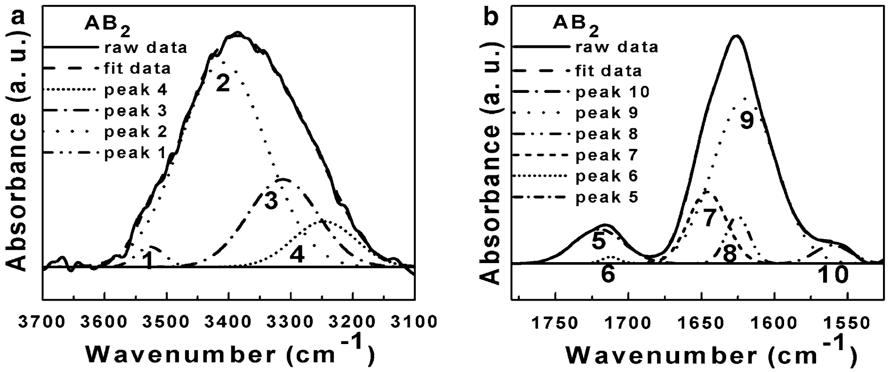

Fig. 1 FT-IR peak separation of AB_2 in 3,700–3,100 cm^{-1} (**a**) and 1,800–1,525 cm^{-1} (**b**) regions

Table 1 FT-IR assignments for characteristic bands of AB_2, HBPEA and HBPEA/RE_2O_3

Samples	Band assignment	Wavenumber (cm^{-1})	Curve fitting calculations
AB_2			
Peak 1	Free O–H hydroxy group	3,526	$A^{a}_{c\ C=O}/A^{b}_{ta,\ C=O,\ C=C} = 0.1218$; $A^{c}_{th,\ O-H}/A^{d}_{tc,\ O-H} = 2.02$; $A_{tc,\ O-H}/A_{t\ O-H} = 0.3306$; $A_{th\ O-H}/A_{t\ O-H} = 0.6694$; $A^{e}_{t\ O-H}/A_{ta,\ C=O,\ C=C} = 0.5368$
Peak 2	H–bonded O–H hydroxy group	3,409	
Peak 3	Free O–H carboxylic group	3,313	
Peak 4	H-bonded O–H carboxylic group	3,246	
Peak 5	Free C=O carboxylic group	1,720	
Peak 6	H-bonded C=O carboxylic group	1,712	
Peak 7	Free C=O amide group	1,646	
Peak 8	Disordered H-bonded C=O amide group	1,625	
Peak 9	Ordered H-bonded C=O amide group	1,620	
Peak 10	C=C group	1,560	
HBPEA			
Peak 11	Free O–H hydroxy group	3,570	$A^{f}_{e\ C=O}/A_{ta,\ C=O,\ C=C} = 0.5142$; $A_{th,\ O-H}/A_{tc,\ O-H} = 2.91$; $A_{t\ O-H}/A_{ta,\ C=O,\ C=C} = 0.5994$
Peak 12	H-bonded O–H hydroxy group	3,433	
Peak 13	H-bonded O–H carboxylic group	3,271	
Peak 14	C=O ester group	1,728	
Peak 15	Free C=O amide group	1,638	
Peak 16	C=C group and H-bonded C=O amide group	1,617	
HBPEA/RE_2O_3			
Peak 17	Free O–H hydroxy group	3,570	$A_{e\ C=O}/A_{ta,\ C=O,\ C=C} = 0.4425$; $A_{th,\ O-H}/A_{tc,\ O-H} = 4.66$; $A_{t\ O-H}/A_{ta,\ C=O,\ C=C} = 0.5544$
Peak 18	H-bonded O–H hydroxy group	3,427	
Peak 19	H-bonded O–H carboxylic group	3,259	
Peak 20	C=O ester group	1,728	
Peak 21	Free C=O amide group	1,637	
Peak 22	C=C group and H-bonded C=O amide group	1,599	

[a] $A_{c\ C=O}$ is the peak area attributed to C=O carboxylic groups

[b] $A_{ta,\ C=O,\ C=C}$ is the addition area of peaks attributed to C=C groups and C=O amide groups

[c] $A_{th,\ O-H}$ is the total peak area attributed to O–H hydroxy groups

[d] $A_{tc,\ O-H}$ is the total peak area attributed to O–H carboxylic groups

[e] $A_{t\ O-H} = A_{tc,\ O-H} + A_{th,\ O-H}$

[f] $A_{e\ C=O}$ is the peak area attributed to C=O ester groups

Figure 3 shows the fitted peaks of IR spectra for HBPEA and HBPEA/RE_2O_3, all the above mentioned absorptions can be identified (showed in Table 1). Comparing with AB_2 monomer, their IR spectra are more intricate owing to the complicated repeat units and branched architectures (see Figs. 1, 3). Based on the spectrum analysis, we can deduce the following results: (1) the overlap between the absorption band of C=C bond at 1,560 cm^{-1} (peak 10) and H-bonded C=O amide group (see peak 16 and 22 in Fig. 3) indicates that the inductive effect is bigger than the conjugative effect in both –C(=O)–C=C–C(=O)– chain structure of HBPEA and HBPEA/RE_2O_3 resulting in the stronger C=C bond strength constant; (2) compared

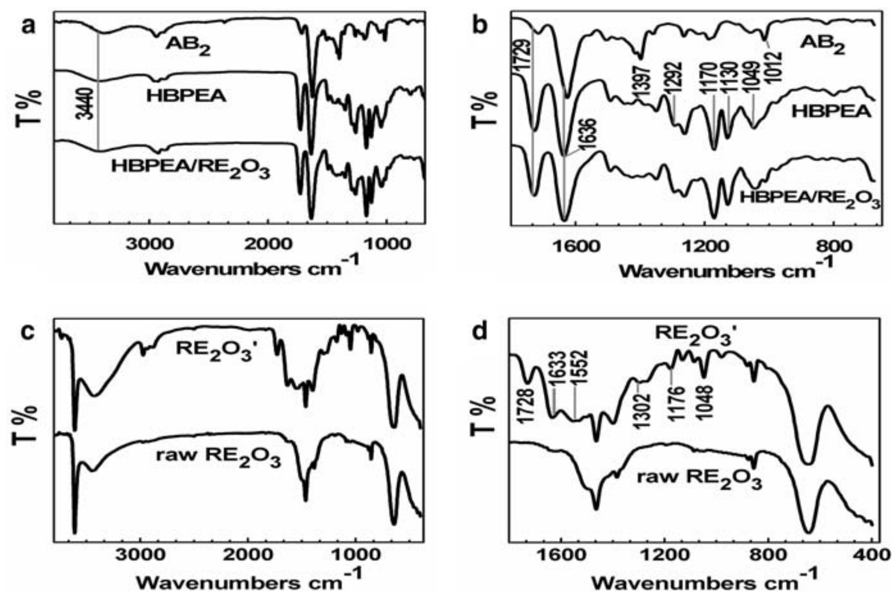

Fig. 2 FT-IR spectra for AB_2, HBPEA and HBPEA/RE_2O_3 (**a**, **b**); RE_2O_3' and raw RE_2O_3 (**c**, **d**)

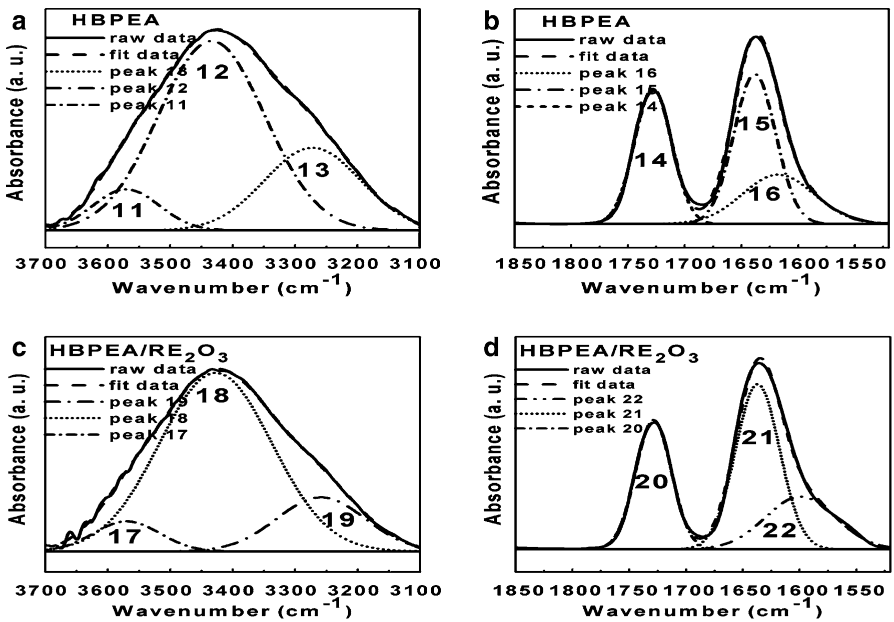

Fig. 3 FT-IR peak separation in the region of 3,700–3,100 cm^{-1} and 1,850–1,520 cm^{-1} for HBPEA (**a**, **b**); HBPEA/RE_2O_3 (**c**, **d**)

peak 22 of HBPEA/RE_2O_3 with peak 16 of HBPEA, a 10 cm^{-1} shift is attributed to the coordinate effect between HBPEA′ and the rare earth ionic (RE^{3+}) which might derive from ionization of RE_2O_3 aggregate surface, and the coordinate effect results in reducing the C=C bond force constant. This maybe imply that it exists the chemical bond interaction between the inorganic RE_2O_3' and organic HBPEA′ in HBPEA/RE_2O_3 composite. In order to prove this deduction, it can be made by extracting the pure RE_2O_3 particles from HBPEA/RE_2O_3 via iterative dissolution/filtration process, the result shows that the pure RE_2O_3 particles cannot be obtained. Figure 2c and d shows the IR spectra of RE_2O_3' and raw RE_2O_3. The absorption bands at 1,728, 1,633, 1,302, 1,176, 1,048 cm^{-1} attributed to the organic HBPEA′ layer on the surface of RE_2O_3' disappear in the IR spectra of raw RE_2O_3, this indicates that it really exists the chemical bond interaction in a certain extend between the inorganic RE_2O_3' and organic HBPEA′ in HBPEA/RE_2O_3 system.

To understand further phase structure between RE_2O_3' and HBPEA′, surface morphologies of HBPEA/RE_2O_3 composites were investigated by SEM. Figure 4 shows the resulting images and the results of particle size analysis, it can be find that RE_2O_3 can dispersed in the organic successive matrix (HBPEA′, see from image b to image i) while it is unharmonious for HBPEA + RE_2O_3 system (see images j), denoting that (1) AB_2 monomer can polycondense on the RE_2O_3 surface under the proposed condition and envelope RE_2O_3 particles in the process of HBPEA/RE_2O_3 preparation, (2) simply blending will easily risk the more aggregation of RE_2O_3. From the inset curve in Fig. 4, we can see that the mean diameter (D_e) of RE_2O_3 particles increases slightly with increasing the amount of RE_2O_3 as the RE_2O_3 content is below 35 wt%. This can attribute to the structure control function of HBPEA′ with multi-branched structure and multi-functional groups [39].

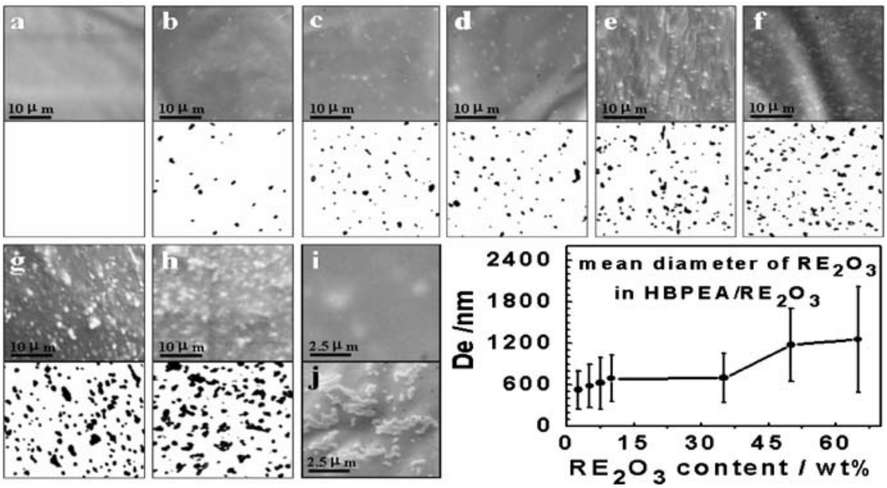

Fig. 4 SEM images of HBPEA (**a**); HBPEA/RE_2O_3 containing 2.5 wt% (**b**), 5 wt% (**c**, **i**), 7.5 wt% (**d**), 10 wt% (**e**), 35 wt% (**f**), 50 wt% (**g**) and 65 wt% (**h**) of RE_2O_3, respectively; HBPEA + RE_2O_3 containing 5 wt% (**j**) of RE_2O_3. The inset exhibits the mean particle diameters of HBPEA/RE_2O_3 composites. Those under the initial images are their threshold binarization

Table 2 The intrinsic viscosity of the HBPEA and HBPEA′

Sample	HBPEA	HBPEA′1	HBPEA′2	HBPEA′3	HBPEA′4
Intrinsic viscosity, η/dL g^{-1}	0.0432	0.0486	0.0471	0.0397	0.0349
$\bar{M}n$/g mol^{-1}	2,031	1,897	2,313	2,013	1,907

HBPEA′1–HBPEA′4 were extracted from HBPEA/RE_2O_3 containing 2.5, 5, 7.5, 10.0 wt% of RE_2O_3, respectively

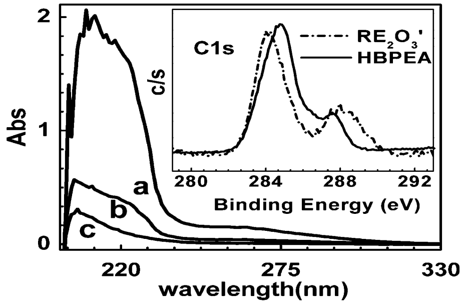

Fig. 5 UV–vis absorption of HBPEA (**a**), HBPEA + RE_2O_3 (**b**) and HBPEA/RE_2O_3 (**c**) in EtOH at room temperature at a concentration of 1×10^{-4} mol/L measured in a 1 cm cuvette. The *inset* shows the comparison of XPS C1s spectra for HBPEA′ and RE_2O_3′

It is well known that the special features of HBP are better solubility and lower solution viscosity due to the branched and denser molecule structure [40]. The intrinsic viscosities and number average molecular weight of HBPEA′ extracted from different HBPEA/RE_2O_3 composites were determined to compare with pristine HBPEA (listed in Table 2). It can be found that the intrinsic viscosities of all HBPEA are very low and there is no difference between these two categorical polymers resulting from the polycondensation of AB_2 monomer with and without RE_2O_3.

To further clarify the structure of HBPEA/RE_2O_3, the UV–vis absorption spectra have been studied as shown in Fig. 5. The high-energy absorption bands at 220–290 nm are assigned to the π–π* transition within –C(=O)–C=C–C(=O)– chain structure in “a” curve [41, 42]. This suggests that carbon–carbon double bonds rooting in MA were not badly destroyed either in the process of AB_2 monomer synthesis or its self-polycondensation to be HBPEA in the case without RE_2O_3 existing. In contrast, it is noted that the absorption ability of the simple blend (HBPEA + RE_2O_3) were drastically decreased though its spectrum (b curve) contains the same absorption range but has less intensity corresponding to that of HBPEA. This reveals that residual nano-scale RE_2O_3 particles incompletely eliminated by filtrating, can influence the feature of HBPEA UV–vis absorption spectrum in a sense [43]. Provided excluding the influence of RE_2O_3 dispersion degree since concentration of the samples are awfully small, it may be the physical adsorption interaction that RE_2O_3 particles can interfere with the absorption ability of HBPEA. However, it is another case for HBPEA/RE_2O_3 composite since there is no visible absorption that can be seen in the corresponding range (c curve), indicating a different influencing mechanism to absorption ability. Change of nearby electronic levels prohibiting charge-transfer transitions [44] may attribute to the main reason to the inactive absorption phenomenon for HBPEA/RE_2O_3 composite, presumably resulting from the coordination between –C(=O)–C=C–C(=O)– chain structure and RE^{3+} derived from ionization of RE_2O_3 aggregate surface. That is, both physical and chemical interaction disturb the absorption ability of HBPEA′ in HBPEA/RE_2O_3 system.

As deduced above, it exists the coordination interaction between –C(=O)–C=C–C(=O)– chain structure and RE^{3+}. This can be further proved by XPS, it was additionally used to determine the surface composition of $RE_2O_3{}'$ extracted from HBPEA/RE_2O_3 (5 wt%) and evaluate their chemical states. A representative survey scan spectrum of $RE_2O_3{}'$ can detect elements: oxygen (530.72 eV), carbon (284.80, 288.79 eV), nitrogen (399.59 eV), lanthanum (834.46, 838.50 eV), cerium (881.53 eV), etc., indicating the thickness of HBPEA′ layer firmly combined with $RE_2O_3{}'$ is smaller than the photoelectron escape depth for there should be no signal of rare earth element provided HBPEA′ layer was thick enough to be pristine HBPEA matrix. In Fig. 5, XPS C1s inset spectra of $RE_2O_3{}'$ (its C 1s was also regarded as that of interfacial HBPEA′ chemically bonding with $RE_2O_3{}'$) and pristine HBPEA (its C1s was regarded as that of interior HBPEA′ segregating with $RE_2O_3{}'$) provide insight as to the nature of the chemical states for carbon atoms of the different HBPEA′ located in HBPEA/RE_2O_3. The 284.80 eV peak is aliphatic hydrocarbon C1s peak, some of which result from contamination. For the comparison between $RE_2O_3{}'$ and HBPEA′, the binding energy of the former is overall shifted to a slightly lower value in 284.00–286.00 eV range but greater in 287.00–288.00 eV range. The slightly lower binding energy for $RE_2O_3{}'$ relative to HBPEA′ may be a result of that the increased electron cloud density of carbon in most of HBPEA′ chain structure, it is due to coordination between –C(=O)–C=C–C(=O)– chain structure and RE^{3+} mentioned above. For the case of higher binding energy, it might result from that electron cloud density of carbon in $(–COO^-)_nRE^{3+}$ ($n = 1, 2, 3,\ldots$) becomes low corresponding to –COOH. Shifted binding energy of other elements on the $RE_2O_3{}'$ surface including oxygen (531.99 → 530.72 eV) and nitrogen (399.37 → 399.59 eV), indicates that the donor atoms participated in coordination are complicated.

Moreover, in order to eliminate the doubt of the ionization and coordination of RE_2O_3 in HBPEA/RE_2O_3 composites, UV–vis transmittance testing experiment was performed as shown Table 3, 480 nm wavelength was selected to exclude the

Table 3 Transmittance of the water solutions(0.5 g/dL) for HBPEA/RE_2O_3 and HBPEA + RE_2O_3

Sample	Transmittance (%)			
	Amount of RE_2O_3 (wt%)			
	2.5	5	7.5	10
HBPEA/RE_2O_3[a]	88.8	42.3	34.1	17.1
HBPEA + RE_2O_3[b]	41.0	24.8	9.9	9.2

[a] Composites of HBPEA and RE_2O_3

[b] Simple blends of HBPEA and RE_2O_3

absorption influence of HBPEA or HBPEA′. In the uniform dispersion suspended system, the suspended particles may induce the light absorbing (particle diameter (D) $\gg$ wavelengh of incidence light (λ)), scattering ($D < \lambda$), reflecting ($D \gg \lambda$), refracting ($D \gg \lambda$), etc. To eliminate the error of dispersion inducing as fully as possible, all specimens were uniformly dispersed by ultrasonic agitation before detecting. The transmittance decreases with increasing the suspended sediment concentrations, since suspended sediment can induce light-passing obstacle and thus decrease transmittance [45]. It is very interesting that all HBPEA/RE_2O_3 composites samples containing RE_2O_3 in the range of 2.5–10 wt% have higher transmittance than HBPEA + RE_2O_3 simple blends with the same RE_2O_3 content. It can be explained by the following reasons: (1) better dispersion and smaller average diameter of RE_2O_3 in HBPEA/RE_2O_3 composites, based on the self-polycondensation of AB_2 monomer and wrapping effect to RE_2O_3; (2) more RE_2O_3 particles in HBPEA + RE_2O_3 simple blends, i.e., the ionization and coordination of RE_2O_3 in HBPEA/RE_2O_3 composites actually occurred while it is not exists in the simple blends of RE_2O_3 and HBPEA.

Up to optimum, there must be only one –COOH group on a theoretical HBPEA molecule while many residual –OH groups surrounding the macromolecular periphery as a three-dimensional spherical shape [46]. But under the synthesis condition selected, it is difficult and unrealistic to realize it. Actually, either HBPEA or HBPEA/RE_2O_3 synthesized in present work possesses handicapped molecule structure with considerable amount of residual -COOH group, proved by curve fitting calculations (Table 1). Distinguishing structure and composition may introduce unique properties. To explore the idea, TGA was employed to comparatively investigate the thermal stability of HBPEA/RE_2O_3 (HBPEA′: $\bar{M}n$ = 2,031, RE_2O_3: 5 wt%), HBPEA + RE_2O_3 (HBPEA: $\bar{M}n$ = 2,313, RE_2O_3: 5 wt%) and HBPEA($\bar{M}n$ = 2,313). Figure 6 depicts the TG and DTG (The inset) curves. It indicates that all of them exhibit multi-stage weight loss with first exothermic decomposition temperature at 224, 212 and 210 °C, respectively, and almost all the weight losses took place in the temperature range of 200–500 °C. The weight loss at below 100, 100–170 and 310–410 °C should be attributed to the release of vapor, residual solvent and water dehydrated, respectively. It can be

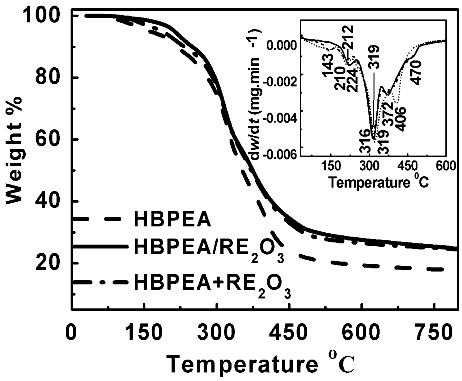

Fig. 6 Thermogravimetric analysis of HBPEA, HBPEA/RE_2O_3 and HBPEA + RE_2O_3. The *inset* shows the corresponding DTG curves

found that the composite-method blending a few RE_2O_3 can achieve a relatively better thermal stability for HBPEA than the simple blending method. Some mechanism that are responsible for inorganic particles enhancing thermal stability of virgin polymer have been suggested, such as “barrier properties of composite” (i.e., “thermal barrier” and “mass transport barrier”, the former protects the polymer from fire, and the latter makes it difficult for degradation products to leave the polymer), “radical trapping” and “physical crosslinking” [47, 48]. In the HBPEA/RE_2O_3 system, the former two mechanisms might be both attributed to the presence of RE_2O_3 and its enhancement for thermal stability. While in HBPEA + RE_2O_3 system, the latter two mechanisms might the main factors to the enhancing thermal stability. It is a matter of fact for RE_2O_3 to continually ionize to be RE^{3+} on suitable condition, especially in temperature elevating case, since a few –COOH in HBPEA/RE_2O_3 composite, which can easily react to RE_2O_3. Rare earth elements have longer atom radius and more coordination numbers, which normally far exceed 6, and thus they possess strong coordination nature. Therefore, during HBPEA pyrolysis, RE^{3+} can interact with unsaturated bond as radical trapper to fix the unstabilized part [49], and also coordinate with the hard-alkali -OH ions to embarrass the dehydration reaction in a certain extent as hard acid. Another thing needs to be emphasized here that the derivative main product in pyrolytic reaction may be a kind of heat-resistant metal-organic compound, according with the result that 12.6% total weight loss of HBPEA/RE_2O_3 occurred above 430 °C and 11.5% for HBPEA + RE_2O_3 system, whereas 8.9% for HBPEA.

Conclusions

Branched polyesteramide/mix rare earth oxides were synthesized by in-situ solution condensation of AB_2 monomer obtained from the reaction between MA and DEA at normal temperature. AB_2 monomer can successfully self-polycondense and form an organic successive matrix of HBPEA′ with a few chemically firm attachment to inorganic RE_2O_3 particle under the proposed condition. The relatively lower intrinsic viscosity was observed for the organic HBPEA′ as well as for the pristine HBEA, which might be due to its multi-branched molecule structure. The firmly bonding between HBPEA′ and RE_2O_3' was assigned to RE^{3+} coordinate with HBPEA′ according to UV–vis and XPS experimental results. In the process of HBPEA/RE_2O_3 synthesis, ionization of RE_2O_3 aggregates surface can produce RE^{3+}. In presence of a few RE_2O_3, thermal stability of HBPEA/RE_2O_3 was significantly improved, it was mainly attributed to “radical trapping” and “mass transport barrier”. To aim at fabricating lower-cost and multifunctional composite material, a feasible and relative simple process was developed for compounding HBPEA and RE_2O_3, this may be regarded as an effective route to produce the new composites.

Acknowledgments The authors acknowledge the financial support from the National Science and Technology Support Project of “the Eleventh Five-year Plan” (2006BAE03B06-03) and the New Century Talents Support Program of Chinese Education Department (NCET-04-0614).

References

1. Mezzenga R, Boogh L, Manson JE (2001) A review of dendritic hyperbranched polymer as modifiers in epoxy composites. Compos Sci Technol 61:787–795
2. Li X, Lu X, Lin Y, Zha J, Li Y, Liu Z, Chen X, Liu S (2006) Synthesis and characterization of hyperbranched poly(ester-amide)s from commercially available dicarboxylic acids and multihydroxyl primary amines. Macromolecules 39:7889–7899
3. Li X, Zhan J, Lin Y, Li Y, Li Y (2005) Facile synthesis and characterization of aromatic and semiaromatic hyperbranched poly(ester-amide)s. Macromolecules 38:8235–8243
4. Li X, Zhan J, Li Y (2004) Facile syntheses and characterization of hyperbranched poly(ester-amide)s from commercially available aliphatic carboxylic anhydride and multihydroxyl primary amine. Macromolecules 37:7584–7594
5. Benthem RATM, Meijerink N, Geladé E, Koster CG, Muscat D, Froehling PE, Hendriks PHM, Vermeulen CJAA, Zwartkruis TJG (2001) Synthesis and characterization of bis(2-hydroxypropyl)amide-based hyperbranched polyesteramides. Macromolecules 34:3559–3566
6. Burkinshaw SM, Froehling PE, Mignanelli M (2002) The effect of hyperbranched polymers on the dyeing of polypropylene fibres. Dyes Pigments 53:229–235
7. Lin Y, Zhang K, Dong Z, Dong L, Li Y (2007) Study of hydrogen-bonded blend of polylactide with biodegradable hyperbranched poly(ester amide). Macromolecules 40:6257–6267
8. Zhang H, He Y, Li S, Liu X (2005) Synthesis and hydrolytic degradation of aliphatic polyesteramides branched by glycerol. Polym Degrad Stab 88:309–316
9. Li X, Su Y, Chen Q, Lin Y, Tong Y, Li Y (2005) Synthesis and characterization of biodegradable hyperbranched poly(ester-amide)s based on natural material. Biomacromolecules 6:3181–3188
10. Kou Y, Wana A, Tong S, Wang L, Tang J (2007) Preparation, characterization and modification of hyperbranched polyester-amide with core molecules. React Funct Polym 67:955–965
11. Cheng X, Huang Z, Liu J, Shi W (2007) Synthesis and properties of semi-crystalline hyperbranched poly(ester-amide) grafted with long alkyl chains used for UV-curable powder coatings. Prog Org Coatings 59:284–290
12. Huang H, Ramaswamy S, Tschirner UW, Ramarao BV (2008) A review of separation technologies in current and future biorefineries. Sep Purif Technol 62:1–21
13. Moisan S, Martinez V, Weisbecker P, Cansell F, Mecking S, Aymonier C (2007) General approach for the synthesis of organic–inorganic hybrid nanoparticles mediated by supercritical CO_2. J Am Chem Soc 129:10602–10606
14. Aymonier C, Schlotterbeck U, Antonietti L, Zacharias P, Thomann R, Tiller JC, Mecking S (2002) Hybrids of silver nanoparticles with amphiphilic hyperbranched macromolecules exhibiting antimicrobial properties. Chem Commun 24:3018–3019
15. Mori H, Boker A, Krausch G, Muller AHE (2001) Surface-grafted hyperbranched polymers via self-condensing atom transfer radical polymerization from silicon surfaces. Macromolecules 34:6871–6882
16. Mu B, Wang T, Liu P (2007) Well-defined dendritic-graft copolymer grafted silica nanoparticle by consecutive surface-initiated atom transfer radical polymerizations. Ind Eng Chem Res 46:3069–3072
17. Mori H, Seng DC, Zhang M, Muller AHE (2002) Hybrid nanoparticles with hyperbranched polymer shells via self-condensing atom transfer radical polymerization from silica surfaces. Langmuir 18:3682–3693
18. Zhao Y, Zou J, Shi W (2005) Synthesis and characterization of PbS/modified hyperbranched polyester nanocomposite hollow spheres at room temperature. Mater Lett 59:686–689
19. Kim SH, Ahn S, Kwak S (2008) Suppression of dioxin emission in incineration of poly(vinyl chloride)(PVC) as hybridized with titanium dioxide (TiO_2) nanoparticles. Appl Catal B Environ 79:296–305
20. Tsetsekou A, Arkas M, Kritikaki A, Simonetis S, Tsiourvas D (2008) Optimization of hybrid hyperbranched polymer/ceramic filters for the efficient absorption of polyaromatic hydrocarbons from water. J Memb Sci 311:128–135
21. Taniguchi Y, Ogawa M, Gang W, Saitoh H, Fujiki K, Yamauchi T, Tsubokawa N (2008) Preparation of hyperfunctional carbon black by grafting of hyperbranched polyester onto the surface. Mater Chem Phys 108:397–402

22. Rhodes SM, Higgins B, Xu Y, Brittain WJ (2007) Hyperbranched polyol/carbon nanofiber composites. Polymer 48:1500–1509
23. Kumari S, Mishra AK, Krishna AVR, Raju KVSN (2007) Organically modified montmorillonite hyperbranched polyurethane–urea hybrid composites. Prog Org Coatings 60:54–62
24. Liu P, Wang T (2007) Preparation of well-defined star polymer from hyperbranched macroinitiator based attapulgite by surface-initiated atom transfer radical polymerization technique. Ind Eng Chem Res 46:97–102
25. Gao C, Yan D (2004) Hyperbranched polymers: from synthesis to applications. Prog Polym Sci 29:183–275
26. Lu H, Yi G, Zhao S, Chen D, Guo L, Cheng J (2004) Synthesis and characterization of multi-functional nanoparticles possessing magnetic, up-conversion fluorescence and bio-affinity properties. J Mater Chem 14:1336–1341
27. Adachi G, Imanaka N, Tamura S (2002) Ionic conducting lanthanide oxides. Chem Rev 102:2405–2429
28. Zhang Z, Lu X, Han B, Luo J (2007) Rare earth effect on the microstructure and wear resistance of Ni-based coatings. Mater Sci Eng A 454–455:194–202
29. Isupova LA, Alikina GM, Snegurenko OI, Sadykov VA, Tsybulya SV (1999) Monolith honeycomb mixed oxide catalysts for methane oxidation. Appl Catal B Environ 21:171–181
30. Santos C, Strecker K, Ribeiro S, Souza JVC, Silva OMM, Silva CRMD (2004) α-SiAlON ceramics with elongated grain morphology using an alternative sintering additive. Mater Lett 58:1792–1796
31. Chen Q, Chen R, Xiao L, Qian Q, Zhang W (2008) Hyperbranched poly(amide-ester) mildly synthesized and its characterization. Chin J Struct Chem 27:877–883
32. Gao C, Yan D (2001) Synthesis of hyperbranched polymers from commercially available A2 and BB'2 type monomers. Chem Commun 1:107–108
33. Benthem RATM (2000) Novel hyperbranched resins for coating applications. Prog Org Coatings 40:203–214
34. Koste S, Duursma MC, Boon JJ, Heeren RMA (2003) Electron capture and collisionally activated dissociation mass spectrometry of doubly charged hyperbranched polyesteramides. J Am Soc Mass Spectrom 14:332–341
35. Muscat D, Henderickx H, Kwakkenbos G, Benthem R, Koster CG (2000) In-source decay of hyperbranched polyesteramides in matrix-assisted laser desorption/ionization time-of-flight mass spectrometry. J Am Soc Mass Spectrom 11:218–227
36. Kaczmarczyk B (1998) FT i.r. study of hydrogen bonds in aliphatic polyesteramides. Polymer 39:5853–5860
37. Rhee H, Lee JS, Lee J, Joo C, Han H, Cho M (2008) Photolytic control and infrared probing of amide I mode in the dipeptide backbone-caged with the 4,5-dimethoxy-2-nitrobenzyl group. J Phys Chem B 112:2128–2135
38. Soon Y, Jun W, Young T, Seung S (2002) Hydrolytic degradation behaviour and microstructural changes of poly(ester-co-amide)s. Polym Degrad Stab 78:63–71
39. Kickelbick G (2003) Concepts for the incorporation of inorganic building blocks into organic polymers on a nanoscale. Prog Polym Sci 28:83–114
40. Yates CR, Hayes W (2004) Synthesis and applications of hyperbranched polymers. Eur Polym J 40:1257–1281
41. Chauhan M, Banerjee K, Arjmand F (2007) DNA binding studies of novel copper(II) complexes containing L-tryptophan as chiral auxiliary: in vitro antitumor activity of Cu–Sn_2 complex in human neuroblastoma cells. Inorg Chem 46:3072–3082
42. Liu L, Ai W, Li M, Liu S (2007) Langmuir-Blodgett films of heteropolyoxometalate/organomercury acetylide hybrid composites: characterization and photoelectric properties. Chem Mater 19:1704–1711
43. Menard LD, Gao S, Xu H, Twesten RD, Harper AS, Song Y, Wang G, Douglas AD, Yang JC, Frenkel AI, Nuzzo RG, Murray RW (2006) Sub-nanometer Au monolayer-protected clusters exhibiting molecule-like electronic behavior: quantitative high-angle annular dark-field scanning transmission electron microscopy and electrochemical characterization of clusters with precise atomic stoichiometry. J Phys Chem B 110:12874–12883
44. Lee D, Donkers RL, Wang G, Harper AS, Murray RW (2004) Electrochemistry and optical absorbance and luminescence of molecule-like Au_{38} nanoparticles. J Am Chem Soc 126:6193–6199

45. Campbell CG, Laycak DT, Hoppes W, Tran NT, Shi FG (2005) High concentration suspended sediment measurements using a continuous fiber optic in-stream transmissometer. J Hydrol 311:244–253
46. Inoue K (2000) Functional dendrimers, hyperbranched and star polymers. Prog Polym Sci 25:453–571
47. Zhu J, Uhl FM, Morgan AB, Wilkie CA (2001) Studies on the mechanism by which the formation of nanocomposites enhances thermal stability. Chem Mater 13:4649–4654
48. Bian L, Qian X, Yin J, Lu Q, Li L, Zhu Z (2002) Preparation and properties of rare earth oxide/polyimide hybrids. Polym Test 21:841–845
49. Zheng Y, Cai W, Fu M, Wang C, Zhang X (2005) Rare earth stearates as thermal stabilizers for rigid poly(vinyl chloride). J Rare Earths 23:172–177